Journal for ImmunoTherapy of Cancer

Degradation of PARP1 by MARCHF3 in tumor cells triggers cCAS-STING activation in dendritic cells to regulate antitumor immunity in hepatocellular carcinoma

Jun Cao,[1,2] Bingbing Su,[1] Chi Zhang,[1,2] Rui Peng,[1] Daoyuan Tu,[1] Qiangwei Deng,[1] Guoqing Jiang,[1] Shengjie Jin,[1] Qian Wang,[1] Dou-Sheng Bai [1,2]

To cite: Cao J, Su B, Zhang C, *et al*. Degradation of PARP1 by MARCHF3 in tumor cells triggers cCAS-STING activation in dendritic cells to regulate antitumor immunity in hepatocellular carcinoma. *Journal for ImmunoTherapy of Cancer* 2024;**12**:e010157. doi:10.1136/jitc-2024-010157

► Additional supplemental material is published online only. To view, please visit the journal online (https://doi.org/10.1136/jitc-2024-010157).

JC, BS, CZ and RP contributed equally.

JC, BS, CZ and RP are joint first authors.

Accepted 26 October 2024

[1]Department of Hepatobiliary Surgery, Northern Jiangsu People's Hospital Affliated to Yangzhou University, Yangzhou City, Jiangsu Province, China
[2]General Surgery Institute, Northern Jiangsu People's Hospital, Yangzhou City, Jiangsu Province, China

Correspondence to
Professor Dou-Sheng Bai; drbaidousheng@yzu.edu.cn

ABSTRACT

Background Resistance to immune checkpoint inhibitors (ICIs) significantly limits the efficacy of immunotherapy in patients with hepatocellular carcinoma (HCC). However, the mechanisms underlying immunotherapy resistance remain poorly understood. Our aim was to clarify the role of membrane-associated ring-CH-type finger 3 (MARCHF3) in HCC within the framework of anti-programmed cell death protein-1 (PD-1) therapy.

Methods MARCHF3 was identified in the transcriptomic profiles of HCC tumors exhibiting different responses to ICIs. In humans, the correlation between MARCHF3 expression and the tumor microenvironment (TME) was assessed via multiplex immunohistochemistry. In addition, MARCHF3 expression in tumor cells and immune cell infiltration were assessed by flow cytometry.

Results MARCHF3 was significantly upregulated in tumors from patients who responded to ICIs. Increased MARCHF3 expression in HCC cells promoted dendritic cell (DC) maturation and stimulated $CD8^+$ T-cell activation, thereby augmenting tumor control. Mechanistically, we identified MARCHF3 as a pivotal regulator of the DNA damage response. It directly interacted with Poly(ADP-Ribose) Polymerase 1 (PARP1) via K48-linked ubiquitination, leading to PARP1 degradation. This process promoted the release of double-strand DNA and activated cCAS-STING in DCs, thereby initiating DC-mediated antigen cross-presentation and $CD8^+$ T-cell activation. Additionally, ATF4 transcriptionally regulated MARCHF3 expression. Notably, the PARP1 inhibitor olaparib augmented the efficacy of anti-PD-1 immunotherapy in both subcutaneous and orthotopic HCC mouse models.

Conclusions MARCHF3 has emerged as a pivotal regulator of the immune landscape in the HCC TME and is a potent predictive biomarker for HCC. Combining interventions targeting the DNA damage response with ICIs is a promising treatment strategy for HCC.

WHAT IS ALREADY KNOWN ON THIS TOPIC

⇒ The anti-programmed cell death protein-1 (PD-1) immunotherapy as the first-line therapy for advanced hepatocellular carcinoma (HCC) has significantly increased the efficacy of cancer treatment. Prior scientific understandings have highlighted the pivotal role of the immune microenvironment in therapeutic efficacy. However, the mechanisms underlying the remodeling of the immune microenvironment in HCC remain to be further elucidated.

WHAT THIS STUDY ADDS

⇒ This study highlights that membrane-associated ring-CH-type finger 3 (MARCHF3) enhances tumor immunogenicity and antitumor immunity through a dendritic cell-T-cell-dependent mechanism by promoting DNA damage in a manner dependent on ATF4, which binds to the promoter of MARCHF3.

HOW THIS STUDY MIGHT AFFECT RESEARCH, PRACTICE OR POLICY

⇒ The data presented in this study provide a rationale for exploring the combination of anti-PD-1 therapy with PARP1-targeted olaparib in clinical trials.

INTRODUCTION

Liver cancer is the sixth most common malignant cancer worldwide and the third leading cause of cancer-related death.[1] Hepatocellular carcinoma (HCC) is the most common pathological type of liver cancer. Approximately half of patients with HCC undergo systemic treatment, predominantly with sorafenib or lenvatinib as the first-line therapy; however, the survival benefits are limited.[2 3] The approval of atezolizumab, an anti-programmed death-ligand 1 (PD-L1) antibody, and bevacizumab, an anti-Vascular Endothelial Growth Factor A (VEGF) antibody, combination treatment as the first-line therapy for advanced HCC has significantly increased the efficacy of cancer treatment.[4] Nevertheless, only approximately 20% of patients with HCC respond to existing immunotherapies, underscoring the need for innovative combination strategies to restore drug

susceptibility in resistant tumors.[5] Additionally, identifying effective biomarkers of the therapeutic response and resistance remains a considerable challenge in guiding patient stratification and treatment selection.

The ubiquitin-proteasome system plays a critical role in regulating protein degradation.[6] E3 ubiquitin ligases are important regulatory factors involved in the development of various cancers.[7] Research has highlighted the involvement of tumor-intrinsic E3 ligases in regulating PD-L1 expression and macrophage infiltration, underscoring the importance of the ubiquitin system in antitumor immunity. Membrane-associated ring-CH-type finger 3 (MARCHF3) belongs to the MARCHF protein family of MARCH ligases.[8–10] Ubiquitination of the interleukin (IL)-6 receptor by MARCHF3 has been reported to inhibit the initiation and progression of colitis-associated cancer.[11] Furthermore, our previous study revealed that MARCHF3 suppresses HCC cell invasion and metastasis by ubiquitinating and degrading GRB2.[12] This observation suggests a potential role for MARCHF3 in HCC development. However, whether MARCHF3 expression in tumors influences antitumor immunity remains largely unexplored.

In this study, we observed the upregulation of MARCHF3 in response to anti-programmed cell death protein-1 (PD-1) therapy, along with its substantial impact on the immune landscape of the HCC microenvironment. Importantly, MARCHF3 ubiquitinated and degraded PARP1, resulting in increased cytosolic double-strand DNA (dsDNA) production. This accumulation, in turn, activated the cGAS-STING signaling pathway in dendritic cells (DCs), leading to the remodeling of the tumor microenvironment (TME) in HCC model mice. These findings provide a theoretical basis for increasing the efficacy of HCC treatment through combination therapy with anti-PD-1 therapy and olaparib.

MATERIALS AND METHODS

Human HCC specimens

HCC was diagnosed using clinical criteria or histology, and the response to treatment was evaluated using the modified Response Evaluation Criteria in Solid Tumors.[13] Patients with HCC classified as having stable disease or a partial response for more than 6 months were categorized as responders, whereas those with progressive disease were deemed non-responders. RNA transcriptome sequencing was conducted on tissue samples from six responders and six non-responders. The tissue microarray was prepared under denaturing conditions, as previously described.[12]

In vivo experiments

6–8-week-old C57BL/6J mice were purchased from the Translational Medical Center at Yangzhou University. $Sting^{-/-}$, $Cgas^{-/-}$, and OT-1 mice were purchased from GemPharmatech. All the mice were bred in SPF-level animal facilities and used in accordance with the guidelines for animal care and use set forth by the Committee on Animal Experimentation. The Animal Utilization Committee of Yangzhou University approved this study. C57BL/6 mice (male, 6–8 weeks old, weighing approximately 19–21 g) were subcutaneously injected with 4×10^6 Hepa1-6 cells resuspended in 100 µL of phosphate-buffered saline (PBS) to induce tumor growth. The tumor volume was determined by measuring the length and width of the subcutaneous tumors using calipers and calculated using the formula (length×width^2)/2. Animals that showed signs of distress or had a maximum tumor diameter >1.5 cm were euthanized. For the orthotopic tumor model, the mice were anesthetized with isoflurane, and 3×10^5 Hepa1-6 cells were inoculated into the liver parenchyma under sterile conditions. For cell injections, a 20 µL suspension of Hepa1-6 cells was mixed with matrix gel and injected into the liver using a microsyringe. Adequate analgesia was provided during and after surgery.

Cells

The MHCC-97H, HUH7, PLC, SK-Hep-1, HCCLM3, Hepa1-6, EMT6, LLC, and Pan02 cell lines were obtained from the Cell Bank of the Chinese Academy of Sciences (CTCC, Shanghai, China). These cell lines were cultured in DMEM (Gibco, USA) supplemented with 10% FBS (Gibco, USA) and 1% penicillin/streptomycin (Thermo) at 37°C in a humidified atmosphere containing 5% CO_2.

Multiplex immunohistochemistry and immunofluorescence staining

All the tissue samples were evaluated by two independent experienced pathologists. Paraffin-embedded human HCC tissues were cut into 5 µm sections for tissue microarray staining. The sections were stained with antibodies against human CD4 (1:200), CD8 (1:200), CD163 (1:200), CD11c (1:200), CD56 (1:200), and MARCHF3 (1:50, Abcam), followed by an incubation with HRP-conjugated anti-mouse or anti-rabbit IgG (Panovue) and a 7-plex IHC kit (PPD 520/540/570/620/650/690/DAPI (Panovue)). Positive cells were detected using the Vectra 3 automated quantitative pathology imaging system (Vectra 3, Akoya Biosciences) and analyzed with inForm software (PerkinElmer).

The cells were cultured on sterile glass coverslips for 48 hours, fixed with 4% paraformaldehyde for 10 min and permeabilized with 0.1% Triton X-100 for 5 min. After blocking for 1 hour, the membranes were sequentially incubated with primary and secondary antibodies. Following the incubation, the cells on the coverslips were washed and mounted with an antifade mounting medium containing DAPI (Beyotime). Images were captured using a fluorescence confocal microscope.

Co-immunoprecipitation and mass spectrometry

Cells were lysed with co-immunoprecipitation (co-IP) buffer containing proteinase, RNase, and phosphatase inhibitors and centrifuged at 12,000 rpm for 8 min to assess the interaction between MARCHF3 and PARP1.

The cell lysate was then incubated with a MARCHF3 antibody for 12 hours, followed by the addition of 50 µL of magnetic beads and further incubation for 3 hours. After the magnetic beads were separated using a magnetic rack, they were washed with PBS and then mixed with SDS sample buffer for western blot analysis. The mass spectrometry (MS) analysis was conducted by GeneChem Biotechnology (China). The antibodies used are listed in online supplemental table 1.

In vivo and in vitro ubiquitination assays

The Flag-MARCHF3, HA-PARP1, and Myc-UB lysine mutant plasmids were transfected into HEK293T cells using a HighGene Transfection reagent (Abclon). 48 hours after transfection, the cells were treated with 10 µM MG132 (MCE) for 6 hours. The cell lysates were subsequently collected. Co-IP experiments were performed with the cell lysates, followed by western blotting to detect ubiquitin and other proteins.

Chromatin immunoprecipitation-qPCR assay

First, 6×10^6 cells were crosslinked with 1% formaldehyde for 10 min and then quenched with 0.2 g of glycine. Chromatin immunoprecipitation (ChIP) was performed using a ChIP kit (Cell Signaling Technology, USA). The chromatin was digested, and the DNA was sonicated to generate 200–800 bp fragments. The cells were incubated with an anti-ATF4 antibody (CST, USA) for 12 hours. The DNA-protein complexes were purified with magnetic beads. The eluted DNA was analyzed by PCR to elucidate whether ATF4 transcriptionally regulated MARCHF3.

Luciferase reporter assay

The experimental plasmids used were pGL4.10, pGL4.10-MARCH3 promoter (WT), pGL4.10-MARCH3 promoter (MUR), pcDNA3.1(+)-MCS-3xFLAG, pcDNA3.1(+)-ATF4-3xFLAG, and pRL-CMV.

The cells were seeded into a 96-well plate at 70% confluence. The cells were transfected with luciferase reporter gene plasmids and transcription factor gene plasmids 24 hours later, with each sample prepared in triplicate wells. For the transfection of plasmids into a 96-well plate, the ratio per well was as follows: firefly luciferase vector/Renilla luciferase vector/transfection reagent=0.1 µg:0.005 µg:0.5 µL. The concentrations of the transcription factor plasmid and control plasmid were 0.1 µg. The DNA and transfection reagent were diluted and incubated at room temperature for 5 min. The diluted DNA and transcription factor vectors were mixed separately with the transfection reagent and incubated at room temperature for 20 min. Then, 50 µL of the medium was removed from each well, and 50 µL of plasmid transfection mixture was added to each well-containing cells. Six hours after transfection, the medium was replaced with a fresh complete culture medium. 48 hours after the cotransfection of plasmids, the culture medium was discarded, and the cells were washed once with 100 µL of 1×PBS. The 96-well plate was removed, and the remaining PBS was aspirated. Next, 5X passive lysis buffer (PLB) was diluted to 1×PLB with deionized water, and the mixture was equilibrated to room temperature before use. Then, 50 µL of diluted 1X PLB was added to each well and shaken on a shaker at room temperature for 15 min to lyse the cells. Subsequently, 5 µL of the supernatant from each step was added to each well of an opaque white 96-well assay plate, followed by the addition of 50 µL of premixed LAR II. The data were collected after 2 s. Then, 50 µL of premixed Stop & Glo Reagent was added to each well, and the data were collected after 2 s of incubation.

Isolation and culture of bone marrow-derived dendritic cells

Bone marrow was extracted from the tibiae and femurs collected from C57BL/6 mice, and the tissues were rinsed with PBS. Bone marrow cells were cultured in RPMI 1640 medium supplemented with 10% FBS, GM-CSF (20 ng/mL), and IL-4 (10 ng/mL) for 6–8 days at 37°C and 5% CO_2 to induce their differentiation into bone marrow-derived dendritic cells (BMDCs).

Flow cytometry analysis

After the experimental mice were anesthetized, they were euthanized, and tumor tissues were collected. The tissues were ground and filtered to obtain a single-cell suspension. Subsequently, immune cells were purified using Percoll gradients (from Sorb, Shanghai). After washes with PBS and counting, approximately 2×10^6 cells were collected as one experimental group for further experiments. The cells were stained with antibodies and Fc-blocking reagents (BioLegend) on ice for 30 min. Staining for intracellular interferon (IFN)-γ and Granzyme B (GZMB) required permeabilization with 0.1% Triton X-100, followed by staining with the antibodies for 90 min. After staining, the samples were analyzed using a Fortessa flow cytometer (BD), and the data were analyzed using FlowJo V.10.6.

Extracellular dsDNA detection

After centrifugation at 5,000 rpm for 5 min at 4°C, the supernatant was collected for dsDNA quantification. According to the manufacturer's protocol, the dsDNA concentration in the supernatant was determined using PicoGreen (Invitrogen).

ELISA

The levels of IFN-γ, GZMB, IFN-β, and CXCL10 in the cell culture supernatants were measured with ELISA kits according to the manufacturer's instructions. The ELISA kits used are listed in online supplemental table 2. The antibodies and primers used are listed in online supplemental table 1.

Statistical analysis

SPSS V.23.0 (IBM, USA) and GraphPad Prism V.9.0 were used to analyze significant differences. Statistical analyses were conducted using a variety of methods. Clinical characteristics were examined using the χ^2 test. Differences between the two groups were assessed using Student's

t-test. Spearman's correlation coefficients were calculated to evaluate correlations. For comparisons among three or more groups, one-way analysis of variance was used. Both single-factor and multifactor Cox regression analyses were employed to identify independent prognostic factors for HCC. Survival rates were assessed using Kaplan-Meier analysis. A p value<0.05 was considered to indicate statistical significance, with *p<0.05, **p<0.01, and ***p<0.001 indicating significance.

RESULTS

MARCHF3 expression influences immunotherapy efficacy and tumorigenesis in HCC

We analyzed the transcriptomic profiles of HCC tumors from patients with varying responses to immune checkpoint inhibitors (ICIs) to explore the impact of E3 ubiquitin ligases on the response of patients with HCC to ICIs. The differentially expressed genes were primarily involved in DC antigen processing and presentation and the response to IFN-γ (figure 1A–C). These findings imply that patients with HCC who are responsive to ICIs generally exhibit immunologically active processes, wherein the regulation of antigen processing and presentation may influence the response of patients with HCC to ICIs. Notably, among a subset of dysregulated E3 ubiquitin ligases (MARCHF3, USP16, RNF130, and TRIM25), MARCHF3 was significantly correlated with immune cell infiltration (online supplemental figure 1 A–D). Additionally, immunohistochemistry (IHC) staining revealed markedly higher levels of MARCHF3 in tumor tissues from responders than in those from non-responders (online supplemental figure 1E). Furthermore, the overexpression of MARCHF3 significantly inhibited tumor growth in mice, particularly after the administration of ICIs, indicating that MARCHF3 overexpression sensitizes tumors to ICIs (figure 1D–F and online supplemental figure 1F–G).

Furthermore, qRT-PCR, western blotting, and IHC staining revealed significantly lower MARCHF3 levels in tumor tissues than in paired peritumoral tissues (figure 1G–J). In our cohort, patients with HCC with high MARCHF3 expression experienced longer overall survival (OS) and disease-free survival (DFS) (figure 1K–L). Furthermore, the multivariate Cox regression analysis revealed that low MARCHF3 expression was an independent adverse predictor of OS and DFS in patients with HCC (figure 1M–N). These findings indicate a close association between MARCHF3 expression and the prognosis, as well as the response of patients with HCC to immunotherapy.

MARCHF3 reshapes the immune landscape of the HCC TME

We subsequently investigated whether changes in MARCHF3 levels can reshape the TME of HCC. Single-sample gene set enrichment analysis (ssGSEA) revealed that patients with HCC in both cohorts with high MARCHF3 expression presented increased immunoreactivity, which is indicative of immunologically "hot" tumors (online supplemental figure 2A–B). MARCHF3 levels were often accompanied by increased lymphocyte infiltration in the TME (online supplemental figure 2C). Additionally, we employed multiplex immunohistochemistry (mIHC) to detect $CD4^+$, $CD8^+$, $CD11c^+$, $CD56^+$, and $CD163^+$ cells in these HCC tissues. The findings revealed that tumors displaying increased MARCHF3 expression levels presented increased infiltration of $CD4^+$ and $CD8^+$ T cells, as well as $CD11c^+$ DCs, whereas no significant differences were detected in the proportions of other immune cells, including $CD56^+$ natural killer (NK) cells and $CD163^+$ macrophages, indicating increased antitumor immunity (figure 2A and online supplemental figure 2D).

Additionally, the flow cytometry analysis revealed the enrichment of $CD8^+$ T and $CD4^+$ T cells in March3-overexpressing tumors (figure 2B). Previous studies have underscored the role of adaptive immune responses in the antitumor effects of immunotherapy.[14] We simultaneously overexpressed March3 and used antibodies to deplete $CD8^+$ or $CD4^+$ T cells to elucidate the specific role of T cells in mediating the antitumor effect of MARCHF3. We found that the depletion of $CD4^+$ T cells had no significant effect on tumor growth, despite March3 overexpression. However, the depletion of $CD8^+$ T cells significantly abrogated the antitumor effect of March3 overexpression (figure 2D–F and online supplemental figure 1H). Considering the important roles of NK cells in antitumor immunity, we also explored whether the antitumor effects of MARCHF3 depend on NK cells. The results showed that NK cell depletion did not affect the tumor-suppressive effects of MARCHF3 (online supplemental figure 2E). Furthermore, the flow cytometry analysis revealed an increased percentage of functional $CD8^+$ T cells ($INF\text{-}\gamma^+CD8^+$; $GZMB^+CD8^+$) in March3-overexpressing tumors (figure 2C and online supplemental figure 2F). Collectively, these findings suggest that $CD8^+$ T cells play a crucial role in mediating the antitumor effects of MARCHF3.

Furthermore, we investigated the impact of MARCHF3 overexpression on $CD8^+$ T cells and established a co-culture model by culturing March3-overexpressing Hepa1-6-OVA cells with $CD8^+$ T cells. However, co-culturing March3-overexpressing Hepa1-6-OVA cells with $CD8^+$ T cells from OT-1 mice did not increase $CD8^+$ T-cell-mediated killing (online supplemental figure 2G). Similarly, in vitro cytotoxicity assays revealed that increasing the levels of March3 in Hepa1-6-OVA cells did not impair the secretion of IFN-γ or GZMB from $CD8^+$ T cells (online supplemental figure 2H–I), suggesting that the overexpression of MARCHF3 did not directly increase $CD8^+$ T-cell activation.

Antigen cross-presentation by DCs or macrophages is the primary mechanism by which tumor-specific $CD8^+$ T cells are activated.[15 16] We depleted DCs in vivo using cytochrome c (Cyt c) and removed macrophages using clodronate liposomes to elucidate the roles of DCs and

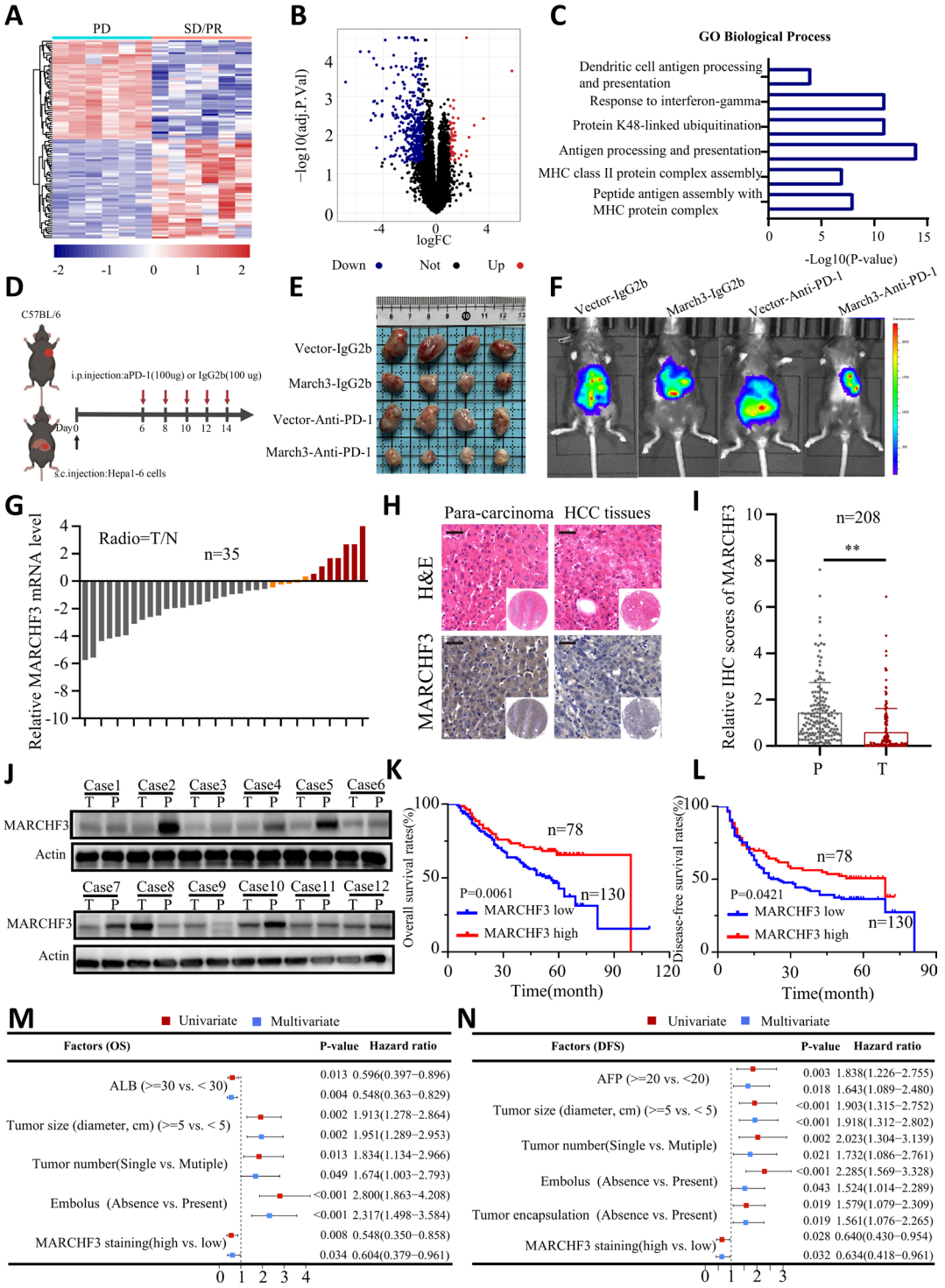

Figure 1 MARCHF3 affects the patient response to ICIs and is correlated with better outcomes. (A) Heatmap showing the differentially expressed genes between responders and non-responders to ICIs. (B) Volcano plot of the differentially expressed genes between ICI responders and non-responders. (C) GO analyses of the DEGs. (D) Scheme of the experimental procedure. (E) Tumor burdens in C57BL/6 mice subcutaneously injected with control vector or March3-overexpressing Hepa1-6 cells and treated with anti-PD-1 antibodies. (F) In vivo imaging systems were used to measure the fluorescence intensity in HCC tumors. (G) The mRNA expression of MARCHF3 in HCC tissues, presented as log(T/N) values. (H–I) Representative image of IHC staining showing MARCHF3 expression in HCC tumors and matched adjacent tissues. Scale bar, 40μm. (J) Protein imprinting analysis revealed the expression of the MARCHF3 protein in HCC tumors and matched adjacent tissues. (K) Kaplan-Meier OS and (L) DFS curves for patients with HCC in the high and low MARCHF3 expression tissue microarray cohorts. (M) Univariate and (N) multivariate analyses of factors associated with OS and DFS. Scale bar: 100 mm (top panel). **p<0.01, Student's t-test. DFS, disease-free survival; GO, Gene Ontology; HCC, hepatocellular carcinoma; ICI, immune checkpoint inhibitor; IHC, immunohistochemistry; MARCHF3, membrane-associated ring-CH-type finger 3; MHC, major histocompatibility complex; mRNA, messenger RNA; OS, overall survival; PD-1, programmed cell death protein-1.

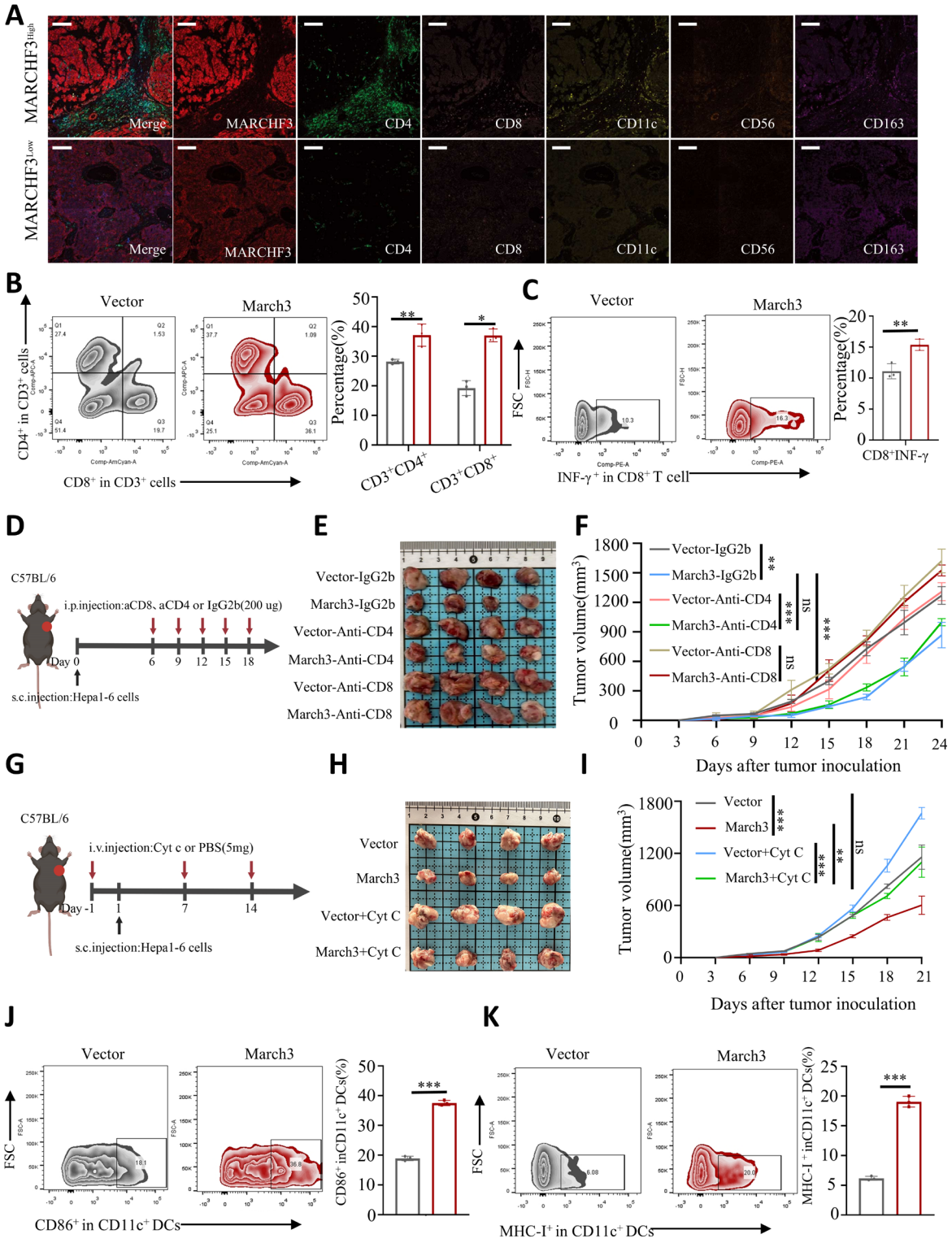

Figure 2 MARCHF3 reshaped the tumor microenvironment by inducing DC maturation and CD8$^+$ T-cell activation. (A) Representative multiplex immunohistochemistry staining results for CD4, CD8, CD11c, CD56, and CD163 in the MARCHF3 high-expression or low-expression groups (scale bar, 50 µm). (B) Flow cytometry analysis of the profiles of infiltrating immune cells, including CD8$^+$ T cells and CD4$^+$ T cells, in tumor tissue. (C) Detection of the cytotoxic activities of CD8$^+$ IFN-γ$^+$ T cells in the MARCHF3 and WT groups by flow cytometry. (D) Schematic representation of the experimental procedure. (E–F) Tumor burdens in C57BL/6 mice subcutaneously injected with tumor cells and administered anti-CD4 or anti-CD8 antibodies. (G) Scheme of the experimental procedure. C57BL6 mice bearing control vector-overexpressing or March3-overexpressing Hepa1-6 tumors were treated with phosphate-buffered saline or Cyt c (depleted DCs). (H) Macroscopic images and (I) average volumes are shown as the means±SDs. n=4 mice per group. (J–K) Flow cytometry analysis of CD86$^+$ CD11c$^+$ DCs (G) and MHC-I$^+$ CD11c$^+$ DCs (H) in the MARCHF3 and WT groups. Cyt c, cytochrome c; DC, dendritic cell; IFN, interferon; MARCHF3, membrane-associated ring-CH-type finger 3; MHC, major histocompatibility complex; WT, wild-type.

macrophages in the antitumor effects of MARCHF3.[17] Intravenous injections of Cyt c successfully eliminated tumor-associated DCs in mice (online supplemental figure 3A–B). Furthermore, the depletion of DCs with Cyt c abolished the inhibitory effect of MARCHF3 expression on tumor growth (figure 2G–I), whereas macrophage depletion did not alter the inhibitory effect (online supplemental figure 3C). These findings indicate that antigen presentation by DCs plays a crucial role in MARCHF3-mediated antitumor activity. Furthermore, the ssGSEA performed in this study revealed that patients with HCC in both cohorts with increased MARCHF3 expression presented elevated DC activation scores (online supplemental figure 3D). Moreover, the flow cytometry analysis further indicated an increased percentage of activated DCs ($CD86^+CD11c^+$; $MHC\text{-}I^+CD11c^+$) in March3-overexpressing tumors (figure 2J–K). Taken together, these results suggest that MARCHF3 can inhibit tumor growth through DC-dependent and $CD8^+$ T-cell-dependent mechanisms.

MARCHF3 suppresses the DNA damage response to activate antitumor immunity

We conducted RNA sequencing analysis to identify differentially expressed genes in tumors overexpressing either March3 or the control vector and to investigate how MARCHF3 regulates tumor cell responses to ICIs. RNA sequencing revealed 1,588 downregulated genes and 802 upregulated genes in March3-overexpressing tumors compared with those in tumors expressing the control vector (figure 3A). Gene Ontology analysis indicated that the dfferentially expressed genes (DEGs) were involved primarily in double-strand break (DSB) repair, myeloid cell differentiation, and T-cell differentiation (figure 3B). Importantly, the pathway enrichment analysis revealed significant activation of the cytosolic DNA-sensing pathway in March3-overexpressing tissues (figure 3C). Notably, disrupted DNA repair may exacerbate DNA damage, particularly DSBs.[18]

Thus, we assessed whether MARCHF3 affects DNA repair. We overexpressed MARCHF3 in Huh7 cells and knocked down MARCHF3 in HCCLM3 cells (online supplemental figure 4A). Western blot and immunofluorescence (IF) analyses confirmed an increase in the level of γH2AX, a sensitive molecular marker of DNA damage and repair, in cells overexpressing MARCHF3 (figure 3D–E and online supplemental figure 4C). Changes in γH2AX focus formation were subsequently measured. 24 hours after the cessation of oxaliplatin (10 µmol/L) treatment, control cells presented significantly fewer γH2AX foci than cells expressing MARCHF3 (figure 3F–G). Moreover, comet assays revealed that DSB repair occurred within 1 hour, while cells overexpressing MARCHF3 accumulated more DSBs (online supplemental figure 4B). DNA damage leads to the accumulation of cytosolic DNA, which serves as the initial factor activating cytoplasmic DNA-sensing pathways.[19] Following dsDNA antibody staining, we observed that overexpression of MARCHF3 increased the amount of cytoplasmic dsDNA in Huh7 cells after oxaliplatin treatment (online supplemental figure 4D). Similarly, dsDNA release into the supernatant was elevated in MARCHF3-overexpressing Huh7 cells (online supplemental figure 4G). However, this effect was reversed by knocking out MARCHF3 (online supplemental figure 4 E–G). In summary, these results suggest that the overexpression of MARCHF3 inhibits the activation of the DSB repair pathway. Additionally, the cGAS-STING pathway is a critical component of the innate immune response activated by pathogenic DNA.[20] DNA derived from tumors can trigger the cGAS/STING pathway, leading to the activation of the IFN-I pathway.[21] Previous research has shown that the cGAS-STING pathway plays a key role in increasing the cross-priming capacity of DCs and activating tumor-specific $CD8^+$ T cells.[22] Therefore, we speculated that MARCHF3 might mediate cGAS-STING activation to regulate antitumor immunity in HCC. We inoculated tumors into $Cgas^{-/-}$ and $Sting^{-/-}$ knockout mice to investigate this possibility. While March3 overexpression effectively controlled tumor growth in wild-type (WT) mice, its effects were completely abrogated in $Cgas^{-/-}$ and $Sting^{-/-}$ mice (figure 4A–C), suggesting an essential role for host cGAS-STING signaling. Since HCC cells exhibit low expression of cGAS (online supplemental table 3), our research focused on the cGAS-STING pathway in DCs.

We next treated vector-overexpressing and March3-overexpressing Hepa1-6 cells with oxaliplatin and co-cultured them with BMDCs for 4 hours. We subsequently isolated DCs and detected cytosolic dsDNA (figure 4D). We observed significant activation of cGAS-STING pathway-related genes, including TBK1 and IRF3, in these BMDCs. However, no changes in the levels of phosphorylated TBK1 or IRF3 were detected in $Cgas^{-/-}$ or $Sting^{-/-}$ mice (figure 4E). Additionally, we detected an increase in dsDNA levels in the DCs of mice overexpressing March3, suggesting that dsDNA from the tumors entered the host DCs (figure 4F).

We extracted BMDCs from WT, $Sting^{-/-}$, and $Cgas^{-/-}$ mice for qRT-PCR, ELISA, and flow cytometry experiments to confirm whether the ability of March3 overexpression to promote the activation of the type I IFN production pathway in DCs depends on cGAS/STING. As expected, following the induction of DNA damage by the overexpression of March3, the messenger RNA (mRNA) expression of Cxcl10, Ifnb, Ccl5, and Isg15 was upregulated in WT BMDCs (online supplemental figure 5A), accompanied by a significant increase in the production of CXCL10 and IFN-β in the cell culture supernatant (figure 4G–H). Interestingly, in the cGAS-deficient mice, no significant changes in the mRNA levels of these genes were observed in either group (figure 4G–H and online supplemental figure 5B). Similar results were also observed in $Sting^{-/-}$ BMDCs (figure 4G–H and online supplemental figure 5C).

We further validated the role of MARCHF3 in DC maturation and $CD8^+$ T-cell activation through cell co-culture experiments. Upregulation of March3 in Hepa1-6 cells led

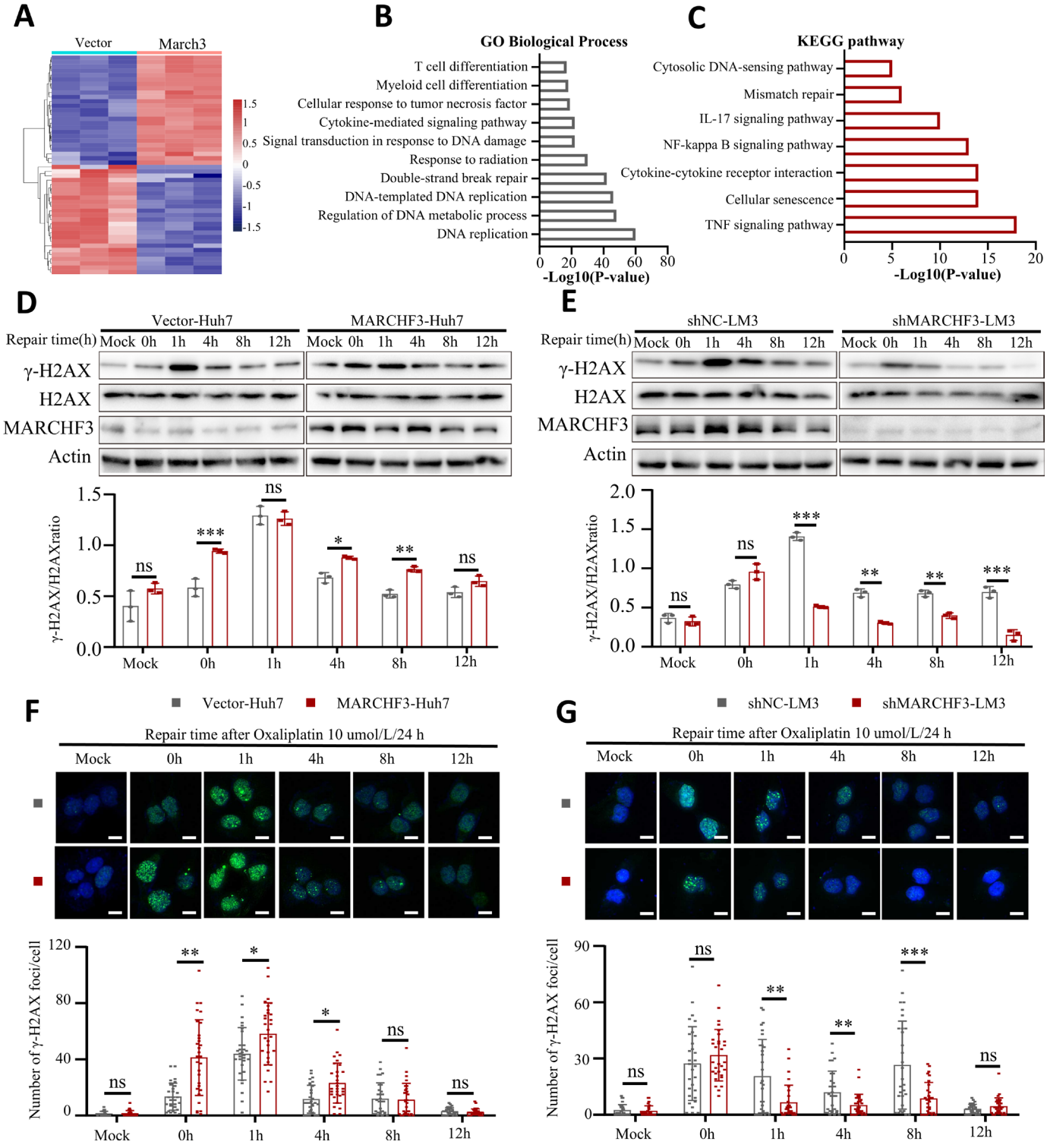

Figure 3 MARCHF3 inhibited DNA repair after DNA damage. (A) Heatmap displaying the differentially expressed genes between vector-treated and MARCHF3-overexpressing tumor tissues. (B) GO and (C) KEGG pathway enrichment analyses of the differentially expressed genes. (D–E) Western blot analysis of rH2AX expression in (D) Huh7 cells and (E) HCCLM3 cells. (F–G) The number of rH2AX foci in (F) Huh7 and (G) HCCLM3 cells. Scale bars, 50 µm. GO, Gene Ontology; IL, interleukin; KEGG, Kyoto Encyclopedia of Genes and Genomes; MARCHF3, membrane-associated ring-CH-type finger 3; TNF, Tumor necrosis factor.

to increased expression of maturation markers, including MHC-I and CD86, on the surface of BMDCs (figure 4I–J and online supplemental figure D). Moreover, the expression of cytotoxic markers, including IFN-γ and GZMB, on the surface of $CD8^+$ T cells increased (figure 4K–L and online supplemental figure 5E). Similarly, we observed no significant differences between March3-overexpressing $Sting^{-/-}$ and $Cgas^{-/-}$ mice (figure 4I–L and online

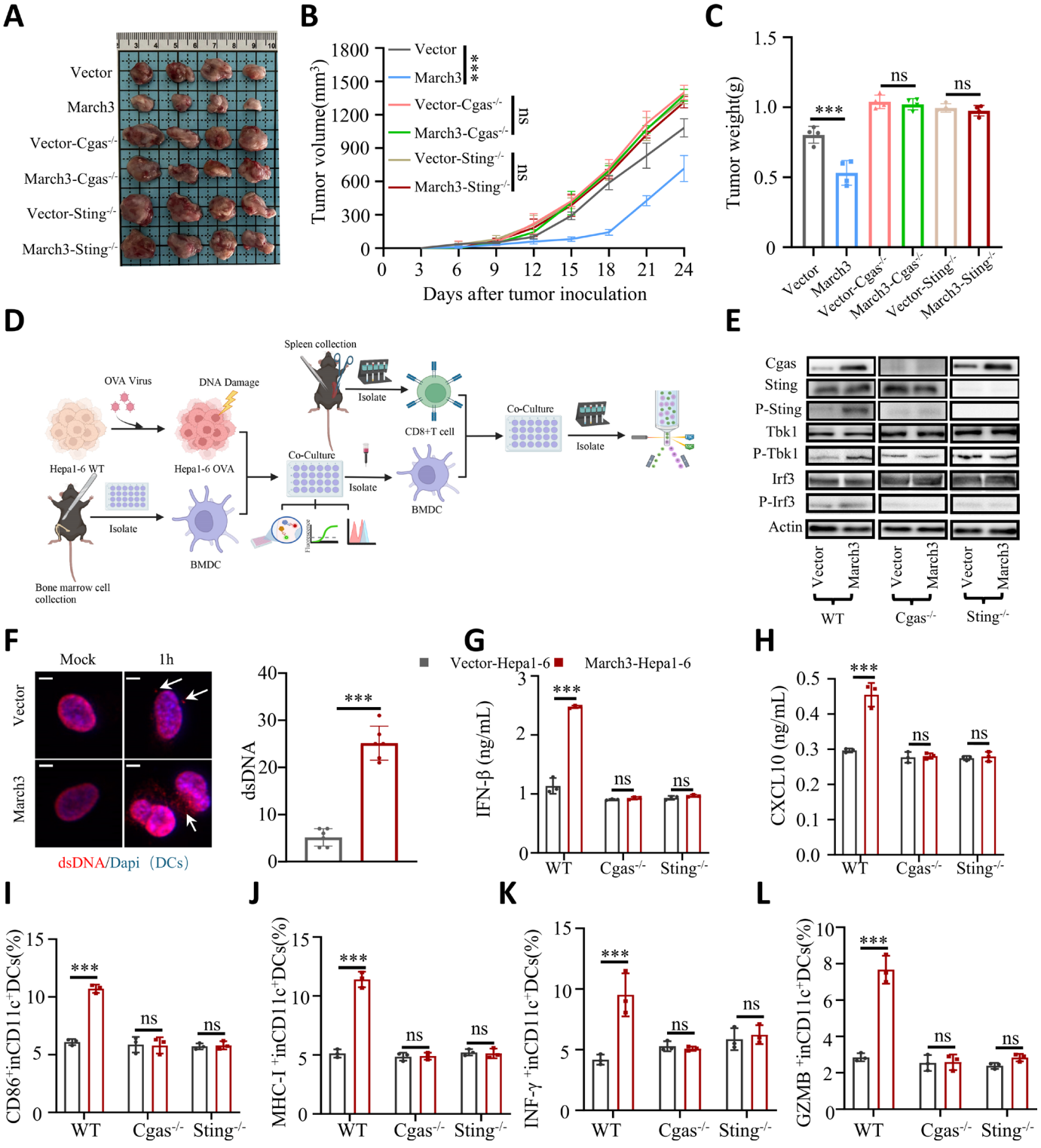

Figure 4 MARCHF3 triggered DC cCAS-STING activation to regulate antitumor immunity in HCC. (A–C) Macroscopic images (A), average tumor volumes (B) and average tumor weights (C) in WT, Cgas–/–, and Sting–/– mice in the MARCHF3 and vector groups. (D) Scheme of the experimental procedure. (E) Western blot analysis was conducted to assess the expression of proteins in the cGAS-STING pathway in DCs from WT, Cgas–/–, and Sting–/– mice. (F) DCs from the WT and MARCHF3 groups were subjected to dsDNA (red) and nuclear (DAPI) immunofluorescence staining. Scale bar, 20μm. (G–H) ELISAs were used to determine the (G) IFN-β and (H) CXCL10 levels in the supernatants of WT, Cgas$^{-/-}$, and Sting$^{-/-}$ mouse DCs. (I–J) FC analysis of (I) CD86^{+} CD11c^{+} DCs and (J) MHC-I^{+} CD11c^{+} DCs from WT, Cgas$^{-/-}$, and Sting$^{-/-}$ mice. (K) IFN-γ^{+} CD8^{+} T cells and (L) GZMB^{+} CD8^{+} T cells among CD8+T cells from WT, Cgas$^{-/-}$, and Sting$^{-/-}$ mice were detected using flow cytometry. BMDC, bone marrow-derived dendritic cell; DAPI, 4',6-diamidino-2-phenylindole; DC, dendritic cell; dsDNA, double-strand DNA; GZMB, Granzyme B; HCC, hepatocellular carcinoma; IFN, interferon; MARCHF3, membrane-associated ring-CH-type finger 3; MHC, major histocompatibility complex; WT, wild-type.

supplemental figure 5D–E). In summary, these data indicate that the overexpression of March3 in Hepa1-6 cells effectively promotes DC maturation and enhances $CD8^+$ T-cell function, leading to increased $CD8^+$ T-cell-mediated killing. Additionally, this process relies on the activation of the cGAS/STING pathway in DCs.

MARCHF3 promotes PARP1 degradation by increasing its K48-linked ubiquitination

We further investigated the molecular mechanisms by which MARCHF3 inhibits the DNA damage response by performing IP-MS to screen for potential molecules interacting with MARCHF3. Interestingly, PARP1 was identified in the list of molecules (figure 5A and online supplemental table 4). Furthermore, PARP1 is known to be a key factor involved in DNA damage repair in tumor cells.[23] Therefore, we believe that PARP1 is a potential target of MARCHF3.

Co-IP and IF analyses revealed that MARCHF3 and PARP1 were both localized in the nuclei of HCC cells (figure 5B–D). Additionally, the results of the GST

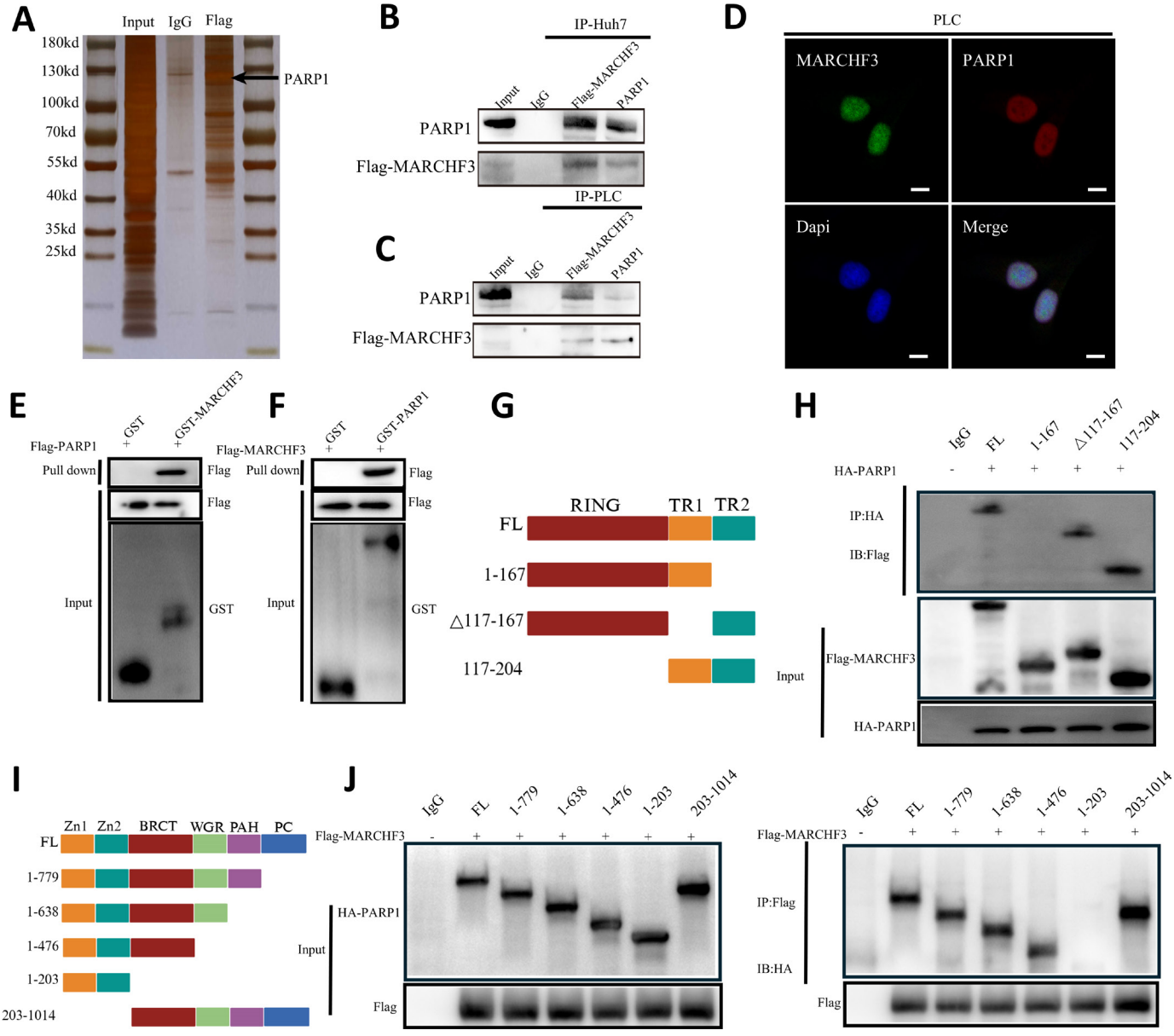

Figure 5 MARCHF3 interacted with PARP1. (A) Silver staining of eluates resolved by SDS-PAGE. (B–C) Co-immunoprecipitation assays showing the interaction of MARCHF3 with PARP1 in (B) Huh7 and (C) PLC cells. (D) Immunofluorescence assays showing the interaction and nuclear colocalization of MARCHF3 with PARP1 in hepatocellular carcinoma cells. Scale bar, 20 µm. (E–F) The interaction between MARCHF3 and PARP1 was assayed via GST precipitation, and purified GST was used as the control. (G) Domain structures of MARCHF3 and the MARCHF3 deletion mutants used in the study. (H) The domain of MARCHF3 that interacts with PARP1. (I) Domain structures of the PARP1 and deletion mutants used in the study. (J) The domain of PARP1 that interacts with MARCHF3.GST, Glutathione-S-transferase; IP, immunoprecipitation; MARCHF3, membrane-associated ring-CH-type finger 3; PARP1, Poly [ADP-ribose] polymerase 1; SDS-PAGE, Sodium dodecyl sulfate polyacrylamide gel electrophoresis.

pulldown assay confirmed a direct interaction between MARCHF3 and PARP1 (figure 5E–F). We subsequently characterized the interaction between MARCHF3 and PARP1. Co-IP assays using truncated MARCHF3 or PARP1 proteins lacking different structural domains revealed that the TR2 domain of MARCHF3 (167–204) is required for binding to PARP1 (figure 5G–H) and that the BRCT domain (203–476) of PARP1 is required for binding to MARCHF3 (figure 5I–J).

Next, considering that MARCHF3 is an E3 ligase, we investigated whether MARCHF3 regulates the degradation of PARP1. The results revealed that MARCHF3 did not affect the PARP1 mRNA level, suggesting that MARCHF3 may regulate the post-translational modification of PARP1 (figure 6A–B). However, PARP1 protein expression decreased in HCC cells with high MARCHF3 expression, whereas MARCHF3 knockdown increased the PARP1 protein level (figure 6C–D). Treatment with the proteasome inhibitor MG132 abrogated the decrease in PARP1 levels induced by MARCHF3 overexpression (figure 6E). Moreover, the downregulation of MARCHF3 resulted in a more significant increase in MG132-induced PARP1 expression (figure 6F). Cycloheximide treatment shortened the half-life of the PARP1 protein in Huh7-MARCHF3 cells (figure 6G), whereas MARCHF3 knockdown stabilized the PARP1 protein in HCCLM3 cells (figure 6H). Additionally, compared with their corresponding control cells, Huh7-MARCHF3 cells presented increased levels of PARP1 ubiquitination (figure 6I), whereas the level of PARP1 ubiquitination decreased in HCCLM3-MARCHF3 cells (figure 6J). Furthermore, mutations in the TR2 domain of MARCHF3 or the BRCT domain of PARP1 reduced the level of ubiquitinated PARP1 (figure 6K–L). We constructed a series of ubiquitin lysine mutants (K6, K11, K27, K29, K33, K48, and K63) and then conducted a ubiquitination analysis to determine the specific type of ubiquitination induced by MARCHF3 (figure 6M). We found that MARCHF3 could ubiquitinate and induce PARP1 degradation by the proteasome by inducing K48-linked ubiquitination (figure 6N). These results suggest that MARCHF3 participates in the ubiquitin-mediated degradation of PARP1.

Overexpression of PARP1 abrogates the antitumor immune effect of MARCHF3 in vitro

We validated the role of MARCHF3 in regulating PARP1 and exerting antitumor immune effects by conducting rescue experiments in which Huh7 or PLC cells were divided into three groups: negative control, MARCHF3, and MARCHF3+PARP1. The results revealed that the overexpression of MARCHF3 increased the formation of γH2AX foci, a hallmark of DNA damage, and the expression of γH2AX in cells treated with oxaliplatin; however, these changes were abrogated by the overexpression of PARP1 (online supplemental figure 6A–D). Comet assays revealed that the level of DNA damage remained high in MARCHF3-overexpressing cells, consistent with delayed DNA repair in MARCHF3-overexpressing cells. Furthermore, the overexpression of PARP1 reversed this DNA damage (online supplemental figure 6E–G). These findings revealed that MARCHF3 regulates the DSB repair process by targeting PARP1 for ubiquitination. Based on the results described above, we constructed a cell co-culture system of Hepa1-6 cells and BMDCs (online supplemental figure 7A). March3 overexpression increased the amount of dsDNA in BMDCs, which was abrogated by PARP1 overexpression (online supplemental figure 7B). Additionally, we found that PARP1 overexpression significantly inhibited the type I IFN production pathway in DCs in a manner dependent on cGAS/STING (online supplemental figure 7C–F), as well as DC maturation and $CD8^+$ T-cell function (online supplemental figure 7G–H). Collectively, these findings indicate that MARCHF3 can promote antitumor immunity through PARP1.

MARCHF3 expression is induced by endoplasmic reticulum stress and is transcriptionally activated by ATF4

We used ssGSEA to compare the hallmark scores of patients with HCC with high and low MARCHF3 expression and to explore the specific regulatory mechanism of MARCHF3. The results revealed a significant positive correlation between MARCHF3 expression and endoplasmic reticulum (ER) stress (online supplemental figure 8A). Given that MARCHF3 is predominantly distributed in the ER, we speculate that a regulatory relationship may exist between ER stress and MARCHF3 expression.[24 25] Neither the upregulation nor the downregulation of MARCHF3 expression in HCC cells affected the mRNA expression levels of ATF4, GRP78, or ATF6 (online supplemental figure 8B–C). Interestingly, we found that thapsigargin and tunicamycin induced an increase in MARCHF3 expression, indicating that ER stress may be among the important causes of the transcriptional activation of MARCHF3 in HCC (online supplemental figure 8D–F). ER stress primarily affects three transcription factors (ATF4, ATF6, and XBP1), which activate downstream effector molecules to counteract stress and restore ER homeostasis.[26] Therefore, we focused on the roles of ATF6, XBP1, and ATF4 in the transcriptional regulation of MARCHF3. A significant positive correlation was detected between MARCHF3 and ATF4 expression, whereas no significant correlation was detected between MARCHF3 and ATF6 or XBP1 expression (online supplemental figure 8G–H). Therefore, we speculate that ATF4 may transcriptionally regulate the expression of MARCHF3. The use of E235 (an ATF4-specific activator) or the overexpression of ATF4 significantly upregulated the expression of MARCHF3 (online supplemental supplemental figure 9A–D). We subsequently performed a bioinformatics analysis to screen four binding sites located in the promoter region of the MARCHF3 gene (online supplemental figure 9E). ChIP confirmed that ATF4 directly bound to site 1 within the MARCHF3 promoter and that the deletion of this site completely attenuated the transcriptional activation of MARCHF3 by ATF4, as revealed by a luciferase assay

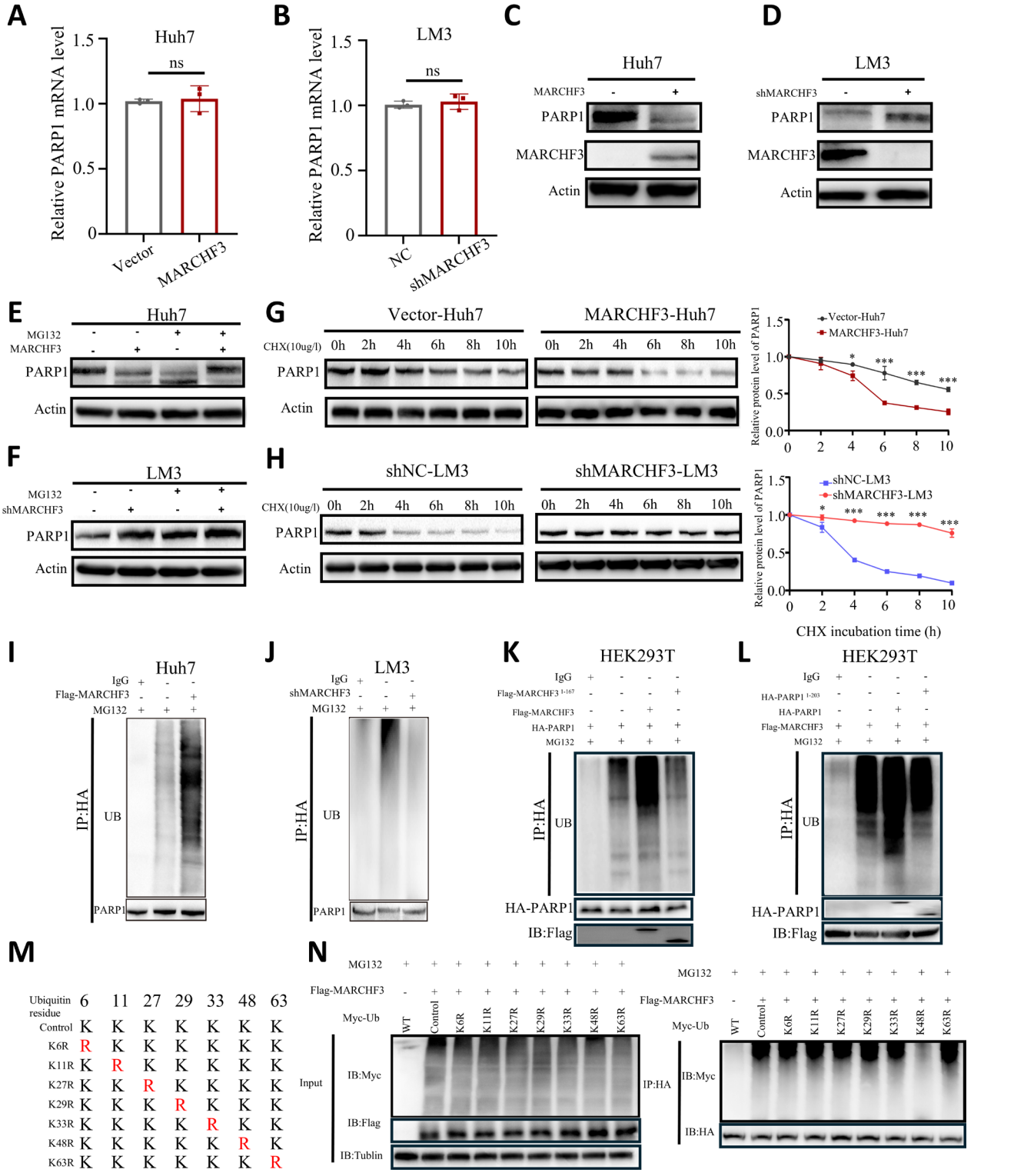

Figure 6 MARCHF3 ubiquitinated PARP1. (A–B) MARCHF3 expression did not affect PARP1 mRNA expression in (A) Huh7-MARCHF3 and (B) HCCLM3-shMARCHF3 cells. (C–D) Western blot analysis of the effect of MARCHF3 on PARP1 protein levels in (C) Huh7 and (D) PLC cells. (E–F) Western blot analysis of PARP1 levels in (E) Huh7-MARCHF3 and (F) HCCLM3-shMARCHF3 cells cultured in the presence of MG132. (G–H) Western blot analysis of the effect of MARCHF3 on the half-life of PARP1 in (G) Huh7-MARCHF3 and (H) HCCLM3-shMARCHF3 cells treated with cycloheximide (10 mg/mL) for the indicated periods. (I–J) Ubiquitination of PARP1 in Huh7-MARCHF3 cells (I) or HCCLM3-shMARCHF3 cells (J) treated for 6 hours with 10 µM MG132. (K–L) Ubiquitination of PARP1 in HEK293T cells transfected with Flag1-176 (K) or HA1-203 (L) and treated for 6 hours with 10 µM MG132. (M) A schematic diagram of MARCHF3 and its mutants. (N) Immunoblotting was used to detect the ubiquitination of PARP1 mutants in HEK293T cells cotransfected with Myc-UB mutants, Flag-MARCHF3, and HA-PARP1. IP, immunoprecipitation; MARCHF3, membrane-associated ring-CH-type finger 3; mRNA, messenger RNA; PARP1, Poly [ADP-ribose] polymerase 1; WT, wild-type.

(online supplemental figure 9F–G). Collectively, these results indicate that ATF4 specifically induces MARCHF3 expression in HCC.

Next, we investigated the correlations among the proteins in the ATF4-MARCHF3-PARP1 axis in tumor tissues from patients with HCC. The results suggested that MARCHF3 expression was significantly positively correlated with ATF4 expression and negatively correlated with PARP1 expression in consecutive sections of HCC tissue from the same patient (online supplemental figure 9H). Overall, ATF4, a transcription factor, upregulates MARCHF3 expression and promotes the ubiquitination of PARP1.

Blocking PARP1 increases the efficacy of anti-PD-1 therapy in HCC mouse models

After revealing the impact of MARCHF3 on the regulation of PARP1 and its implications for antitumor immunity, we investigated the clinical significance of targeting PARP1 to reshape the immune microenvironment of HCC. In subcutaneous and orthotopic model mice, the groups treated with both olaparib (a PARP inhibitor) combined with anti-PD-1 therapy presented significant tumor suppression compared with the control, olaparib alone, and anti-PD-1 alone groups (figure 7A–C). Interestingly, we also investigated the clinical value of combination therapy in breast cancer, lung cancer, and pancreatic cancer and obtained results similar to those observed in HCC (online supplemental figure 1A–C). The results of our study are consistent with those of previous reports.[27–29] Moreover, the mIHC results revealed that olaparib increased $CD11c^+$ DC and $CD8^+$ T-cell infiltration (figure 7D). Similarly, flow cytometry experiments confirmed the restoration of DC maturation and improvement in $CD8^+$ T-cell function after olaparib treatment (figure 7E–F).

Here, we demonstrated that in HCC, ATF4 transcriptionally upregulates MARCHF3 expression, thereby promoting PARP1 ubiquitination. Inhibition of PARP1 suppresses DNA damage repair in liver cancer cells, while tumor-derived dsDNA activates the cGAS/STING pathway in DCs, further promoting DC maturation and improving the function of cytotoxic $CD8^+$ T cells (figure 7G).

DISCUSSION

Patients with advanced HCC often exhibit poor responses to immunotherapy and poor outcomes. Therefore, a deeper understanding of the specific mechanisms underlying immune evasion in HCC is crucial for increasing the efficacy of immunotherapy for HCC. In this study, we aimed to elucidate the role of E3 ubiquitin ligases in reshaping the immune microenvironment of HCC. While previous evidence has highlighted E3 ubiquitin ligases as key regulators of tumor progression and immune responses,[30–32] their potential contributions to cancer immune evasion mechanisms remain poorly understood.

Through an analysis of the HCC tumor transcriptomic profiles of patients who responded differently to ICIs, we observed the significant upregulation of MARCHF3 in patients with HCC who responded to immunotherapy. Furthermore, we found that MARCHF3 expression in tumor cells impacts hepatocarcinogenesis in an immune-dependent manner. Previous studies have highlighted the role of MARCHF3 in effectively suppressing tumor cell proliferation, invasion, and apoptosis in HCC and colorectal carcinoma through MAPK and STAT3 signaling.[11 12]

However, whether MARCHF3 acts as an immunomodulatory factor that exerts antitumor effects requires further investigation. In this study, we observed that MARCHF3 exerts antitumor effects through DC-mediated T-cell immunity. Previous studies have shown that DCs activate functional $CD8^+$ T cells through antigen presentation, thus eliciting anticancer immune responses.[33] Therefore, reactivating DCs in the TME to promote antitumor effects holds great clinical value. DCs can be subdivided into conventional DCs (cDCs, including the $CD8\alpha^+$ and/or $CD103^+$ cDC1 subset and the $CD11b^+$ cDC2 subset), plasmacytoid DCs (pDCs, $CD11^-$ $B220^+$), and monocyte-derived DCs ($CD14^+$ $CD206^+$).[34] Among them, cDC1s can cross-present antigens to $CD8^+$ T cells, thereby promoting antitumor immunity.[35] Similarly, we found that, compared with low MARCHF3 expression, high MARCHF3 expression in tumor-bearing mice led to increased numbers of infiltrating $CD86^+$ $CD11c^+$ DCs. Furthermore, the depletion of cDC1s in mice abrogated the antitumor effect mediated by MARCHF3, suggesting that cDC1s play a crucial role in MARCHF3-mediated antitumor immunity. Other studies have similarly shown that tumor-derived cDC1 antigen presentation to $CD8^+$ T cells contributes to tumor immunity.[36]

The cGAS-STING pathway is a crucial type I IFN response pathway. When cGAS binds to dsDNA in the cytoplasm, it synthesizes cyclic GMP-AMP, which then binds to and activates the adaptor STING. The activation of this protein initiates a cascade of signaling events, resulting in the release of IFNs and other immune molecules.[37 38] In addition, DNA damage or genomic instability is an important mechanism of cGAS activation. DNA damage leads to the formation of dsDNA, which in turn activates the cGAS-STING pathway.[39] Our data confirmed that MARCHF3 expression inhibits the DNA damage repair process in HCC cells, thereby increasing dsDNA production. Subsequently, tumor-derived dsDNA activates the cGAS-STING pathway in DCs, ultimately activating DCs and improving $CD8^+$ T-cell function. Tumors with disrupted DNA damage repair exhibit stronger DC-mediated cross-activation of $CD8^+$ T cells. Various treatments, such as chemotherapy, radiotherapy, and targeted therapies aimed at DNA repair pathways, can induce DNA damage, leading to activation of the cGAS-STING signaling pathway.[40 41]

Various E3 ubiquitin ligases, such as USP7, USP22, and USP28, are implicated in tumorigenesis and DNA damage processes.[42–44] For example, TRIM25 promotes the

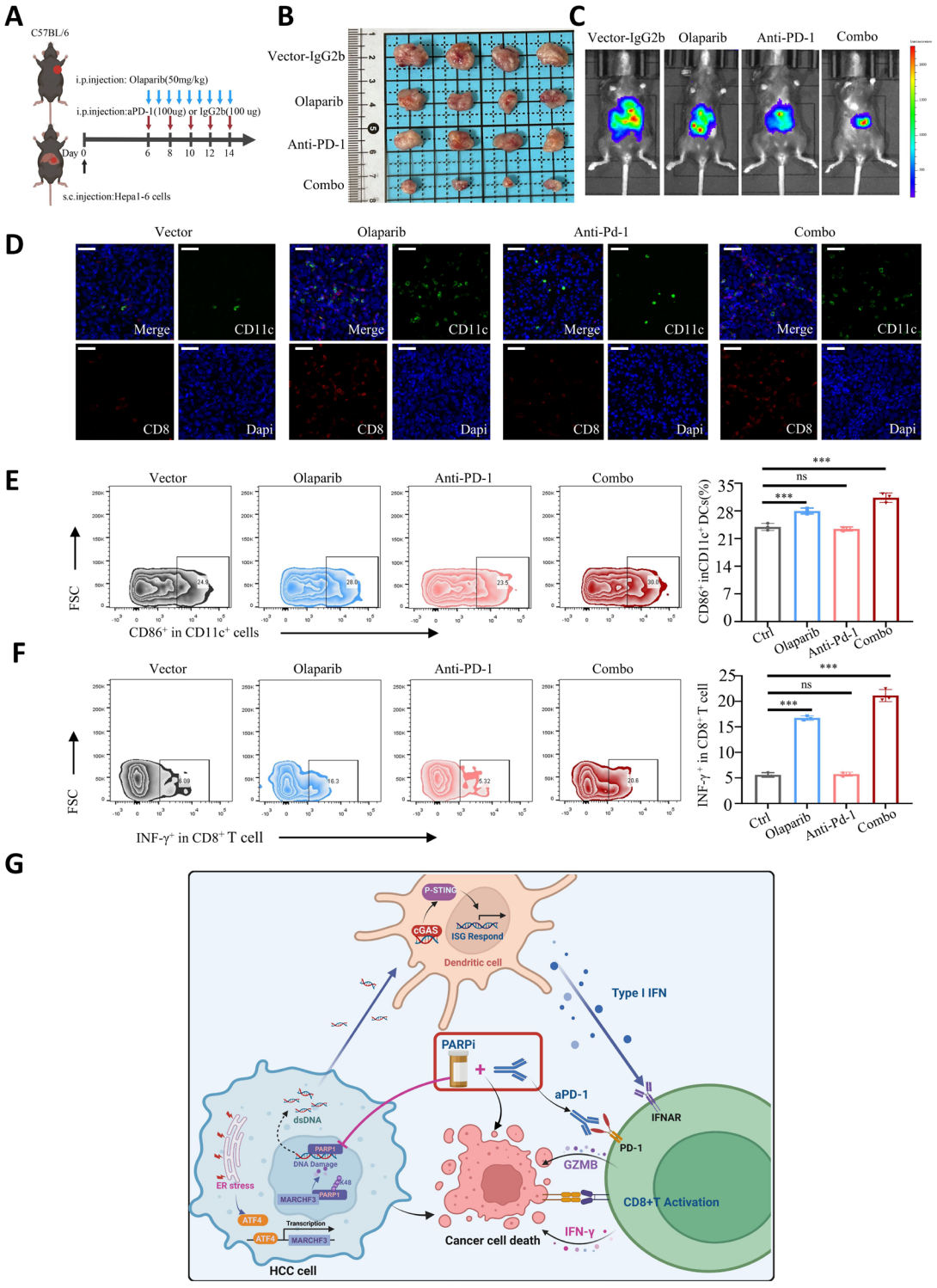

Figure 7 Blockade of PARP1 potentiated the efficacy of anti-PD-1 therapy in HCC. (A) Schematic showing the schedule of treatment with the anti-PD-1 antibody and the PARP1 inhibitor olaparib in the HCC model C57BL/6 mice. (B) Subcutaneous tumor xenografts in mice. (C) In vivo imaging systems were used to measure the fluorescence intensity in HCC tumors. (D) Representative images of multiplex immunohistochemistry staining for CD11c and CD8 in orthotopic HCC tissues. Scale bars, 30 µm. (E–F) Flow cytometry analysis of the proportions of infiltrating (E) $CD86^+$ $CD11c^+$ DCs and (F) $INF\text{-}\gamma^+CD8^+$ T cells in xenograft HCC tissues from each group. (G) ATF4 induced MARCHF3 expression on ER stress. Increased MARCHF3 expression inhibits PARP1-mediated DNA repair that induces DNA damage and cytoplasmic dsDNA release, leading to DC cGAS/STING-dependent activation of type I IFN signaling and thereby reprogramming of the tumor microenvironment. Targeting the DNA damage pathway, such as with the PARP1 inhibitor olaparib. Immune checkpoint inhibitor efficacy against HCC is potentiated. DC, dendritic cell; dsDNA, double-strand DNA; ER, endoplasmic reticulum; GZMB, Granzyme B; HCC, hepatocellular carcinoma; IFN, interferon; MARCHF3, membrane-associated ring-CH-type finger 3; PARP1, Poly [ADP-ribose] polymerase 1; PARPi, PARP inhibitors; PD-1, programmed cell death protein-1.

degradation of Ku80, hindering its recruitment to DNA DSBs. Our study revealed that MARCHF3 overexpression facilitates the degradation of the PARP1 protein via K48-linked polyubiquitin chain formation. PARP1, a nuclear protein, plays a role in the classical non-homologous end joining pathway by interacting with DNA-PKcs and recruiting XRCC4/CHD2 to DSB sites.[45] Interestingly, previous studies have reported that the MARCH E3 ligase family directly targets molecules in the cGAS-STING pathway. For example, recent research has shown that MARCH5 ubiquitinates and degrades STING at K63 ubiquitin sites to inhibit type I IFN responses. Additionally, MARCH8 ubiquitinates CGAS at K63 ubiquitin sites to suppress the cGAS-STING pathway.[46 47] Thus, although members of the MARCH E3 ligase family share similar domains, they exert their effects in markedly different ways. These differences are likely due to differences in the domains of MARCH E3 ligases that interact with target proteins and the specific ubiquitin sites involved. This finding also suggests that the binding and ubiquitination of PARP1 by MARCH3 may have a certain degree of specificity.

PARP1 inhibitors exert antitumor effects on BRCA-deficient triple-negative breast cancer by activating the cGAS-STING pathway.[46] This clinical finding has also been corroborated by other studies.[47] Targeting innate antitumor immunity in combination with PD-1 therapy has emerged as a potentially valuable treatment approach. In our study, we demonstrate that targeting PARP1 effectively increases the efficacy of immunotherapy for HCC. The optimal antitumor effects observed with the combination therapy on preclinical models validate this approach. Furthermore, in addition to activating $CD8^+$ T cells by enhancing antigen presentation through DCs to suppress tumor growth, our research results also indicate that targeting PARP1 can provide a theoretical basis for future combination therapies with anti-PD-1 agents, potentially expanding the application value of PARP1 inhibitors in immunotherapy for HCC.

In summary, our findings suggest that MARCHF3 enhances tumor immunogenicity and antitumor immunity through a DC-T-cell-dependent mechanism by promoting DNA damage in a manner dependent on ATF4, which binds to the promoter of MARCHF3. Upregulated MARCHF3 suppresses PARP1-mediated DNA repair, further activating cGAS-STING pathway-mediated antitumor immunity and thereby sensitizing HCC to ICIs. Consequently, targeting PARP1 in combination with immune checkpoint inhibition represents a promising opportunity for cancer immunotherapy. The potential application of such combination therapy extends beyond HCC and may benefit patients with various types of cancer that do not respond to the available treatments.

Acknowledgements We kindly thank the Yangzhou University Animal Facility staff for their assistance with the breeding and maintenance of the mice used in this study.

Contributors D-SB, JC, BS, CZ and RP designed the study. D-SB is guarantor of the work. JC, BS, CZ and RP collected and analyzed the data. JC, BS, CZ and RP interpreted the data and discussed the conclusions. DT and QD provided bioinformatics support and generated the heatmap. GJ, SJ and QW provided consultations on clinical relevance and the sequence of therapies. JC wrote the manuscript, which all authors critiqued.

Funding This work was funded by the National Natural Science Foundation of China (82373034 and 82203716), the "13th Five-Year Plan" Science and Education Strong Health Project Innovation Team of Yangzhou (LJRC20181 and YZCXTD201801), the Provincial-Level Discipline Leader of the NJPH (DTRA202214), the Cross-Cooperation Special Projects of the NJPH (YJCHZ-2021-08), the Beijing iGanDan Foundation (GDXZ-08-19), and the Postgraduate Research and Practice Innovation Program of Jiangsu Province (KYCX22_3568, KYCX23_3617, and SJCX23_2028), Yangzhou Basic Research Program (Joint Special Project) (2024-3-02).

Competing interests No, there are no competing interests.

Patient consent for publication Not applicable.

Ethics approval The use of the aforementioned hepatocellular carcinoma samples was approved by the Ethics Committee of Subei People's Hospital of Jiangsu Province (ID:2022ky0222), and patient consent was obtained. We have already uploaded the original ethical consent form of our unit in the supplementary materials.

Provenance and peer review Not commissioned; externally peer reviewed.

Data availability statement Data are available upon reasonable request.

ORCID iD

Dou-Sheng Bai http://orcid.org/0000-0001-8032-7959

REFERENCES

1 Siegel RL, Miller KD, Wagle NS, *et al*. Cancer statistics, 2023. *CA Cancer J Clin* 2023;73:17–48.
2 El-Serag HB. Hepatocellular carcinoma. *N Engl J Med* 2011;365:1118–27.
3 Kudo M, Finn RS, Qin S, *et al*. Lenvatinib versus sorafenib in first-line treatment of patients with unresectable hepatocellular carcinoma: a randomised phase 3 non-inferiority trial. *The Lancet* 2018;391:1163–73.
4 Rimini M, Persano M, Tada T, *et al*. Real-World Data for Atezolizumab Plus Bevacizumab in Unresectable Hepatocellular Carcinoma: How Does Adherence to the IMbrave150 Trial Inclusion Criteria Impact Prognosis? *Target Oncol* 2023;18:221–33.
5 Pinter M, Scheiner B, Pinato DJ. Immune checkpoint inhibitors in hepatocellular carcinoma: emerging challenges in clinical practice. *Lancet Gastroenterol Hepatol* 2023;8:760–70.
6 Damgaard RB. The ubiquitin system: from cell signalling to disease biology and new therapeutic opportunities. *Cell Death Differ* 2021;28:423–6.
7 Sampson C, Wang Q, Otkur W, *et al*. The roles of E3 ubiquitin ligases in cancer progression and targeted therapy. *Clin Transl Med* 2023;13:e1204.
8 De S, Holvey-Bates EG, Mahen K, *et al*. The ubiquitin E3 ligase FBXO22 degrades PD-L1 and sensitizes cancer cells to DNA damage. *Proc Natl Acad Sci U S A* 2021;118:e2112674118.
9 Wang X, Tokheim C, Gu SS, *et al*. In vivo CRISPR screens identify the E3 ligase Cop1 as a modulator of macrophage infiltration and cancer immunotherapy target. *Cell* 2021;184:5357–74.

10 Wang X, Herr RA, Hansen T. Viral and cellular MARCH ubiquitin ligases and cancer. *Semin Cancer Biol* 2008;18:441–50.
11 Lin H, Feng L, Cui K-S, *et al*. The membrane-associated E3 ubiquitin ligase MARCH3 downregulates the IL-6 receptor and suppresses colitis-associated carcinogenesis. *Cell Mol Immunol* 2021;18:2648–59.
12 Zhou J, Tu D, Peng R, *et al*. RNF173 suppresses RAF/MEK/ERK signaling to regulate invasion and metastasis via GRB2 ubiquitination in Hepatocellular Carcinoma. *Cell Commun Signal* 2023;21:224.
13 Schwartz LH, Litière S, de Vries E, *et al*. RECIST 1.1—Update and clarification: From the RECIST committee. *Eur J Cancer* 2016;62:132–7.
14 Sharma P, Hu-Lieskovan S, Wargo JA, *et al*. Primary, Adaptive, and Acquired Resistance to Cancer Immunotherapy. *Cell* 2017;168:707–23.
15 Del Prete A, Salvi V, Soriani A, *et al*. Dendritic cell subsets in cancer immunity and tumor antigen sensing. *Cell Mol Immunol* 2023;20:432–47.
16 Ma S, Sun B, Duan S, *et al*. YTHDF2 orchestrates tumor-associated macrophage reprogramming and controls antitumor immunity through $CD8^+$ T cells. *Nat Immunol* 2023;24:255–66.
17 Lin ML, Zhan Y, Proietto AI, *et al*. Selective suicide of cross-presenting CD8+ dendritic cells by cytochrome c injection shows functional heterogeneity within this subset. *Proc Natl Acad Sci U S A* 2008;105:3029–34.
18 Huang R, Zhou P-K. DNA damage repair: historical perspectives, mechanistic pathways and clinical translation for targeted cancer therapy. *Signal Transduct Target Ther* 2021;6:254.
19 Yu L, Liu P. Cytosolic DNA sensing by cGAS: regulation, function, and human diseases. *Signal Transduct Target Ther* 2021;6:170.
20 Woo S-R, Fuertes MB, Corrales L, *et al*. STING-Dependent Cytosolic DNA Sensing Mediates Innate Immune Recognition of Immunogenic Tumors. *Immunity* 2014;41:830–42.
21 Kwon J, Bakhoum SF. The Cytosolic DNA-Sensing cGAS-STING Pathway in Cancer. *Cancer Discov* 2020;10:26–39.
22 Mender I, Zhang A, Ren Z, *et al*. Telomere Stress Potentiates STING-Dependent Anti-tumor Immunity. *Cancer Cell* 2020;38:400–11.
23 Pandey N, Black BE. Rapid Detection and Signaling of DNA Damage by PARP-1. *Trends Biochem Sci* 2021;46:744–57.
24 Fenech EJ, Lari F, Charles PD, *et al*. Interaction mapping of endoplasmic reticulum ubiquitin ligases identifies modulators of innate immune signalling. *Elife* 2020;9:e57306.
25 Neutzner A, Neutzner M, Benischke A-S, *et al*. A systematic search for endoplasmic reticulum (ER) membrane-associated RING finger proteins identifies Nixin/ZNRF4 as a regulator of calnexin stability and ER homeostasis. *J Biol Chem* 2011;286:8633–43.
26 Chen X, Shi C, He M, *et al*. Endoplasmic reticulum stress: molecular mechanism and therapeutic targets. *Sig Transduct Target Ther* 2023;8:352.
27 Jiao S, Xia W, Yamaguchi H, *et al*. PARP Inhibitor Upregulates PD-L1 Expression and Enhances Cancer-Associated Immunosuppression. *Clin Cancer Res* 2017;23:3711–20.
28 Sen T, Rodriguez BL, Chen L, *et al*. Targeting DNA Damage Response Promotes Antitumor Immunity through STING-Mediated T-cell Activation in Small Cell Lung Cancer. *Cancer Discov* 2019;9:646–61.
29 Wang Y, Zheng K, Xiong H, *et al*. PARP Inhibitor Upregulates PD-L1 Expression and Provides a New Combination Therapy in Pancreatic Cancer. *Front Immunol* 2021;12:762989.
30 Meng X, Liu X, Guo X, *et al*. FBXO38 mediates PD-1 ubiquitination and regulates anti-tumour immunity of T cells. *Nature New Biol* 2018;564:130–5.
31 Shembade N, Harhaj NS, Parvatiyar K, *et al*. The E3 ligase Itch negatively regulates inflammatory signaling pathways by controlling the function of the ubiquitin-editing enzyme A20. *Nat Immunol* 2008;9:254–62.
32 Lyle C, Richards S, Yasuda K, *et al*. c-Cbl targets PD-1 in immune cells for proteasomal degradation and modulates colorectal tumor growth. *Sci Rep* 2019;9:20257.
33 Fu C, Jiang A. Dendritic Cells and CD8 T Cell Immunity in Tumor Microenvironment. *Front Immunol* 2018;9:3059.
34 Satpathy AT, Wu X, Albring JC, *et al*. Re(de)fining the dendritic cell lineage. *Nat Immunol* 2012;13:1145–54.
35 Sánchez-Paulete AR, Teijeira A, Cueto FJ, *et al*. Antigen cross-presentation and T-cell cross-priming in cancer immunology and immunotherapy. *Ann Oncol* 2017;28:xii44–55.
36 Liu H, Golji J, Brodeur LK, *et al*. Tumor-derived IFN triggers chronic pathway agonism and sensitivity to ADAR loss. *Nat Med* 2019;25:95–102.
37 Goedegebuure RSA, Kleibeuker EA, Buffa FM, *et al*. Interferon- and STING-independent induction of type I interferon stimulated genes during fractionated irradiation. *J Exp Clin Cancer Res* 2021;40:161.
38 Chen J, Zhao B, Dong H. Inhibition of o-glcnac transferase activates type i interferon-dependent antitumor immunity by bridging cgas-sting pathway. *Cancer Biology* [Preprint].
39 Li T, Chen ZJ. The cGAS-cGAMP-STING pathway connects DNA damage to inflammation, senescence, and cancer. *J Exp Med* 2018;215:1287–99.
40 Pantelidou C, Sonzogni O, De Oliveria Taveira M, *et al*. PARP Inhibitor Efficacy Depends on $CD8^+$ T-cell Recruitment via Intratumoral STING Pathway Activation in BRCA-Deficient Models of Triple-Negative Breast Cancer. *Cancer Discov* 2019;9:722–37.
41 Shen J, Zhao W, Ju Z, *et al*. PARPi Triggers the STING-Dependent Immune Response and Enhances the Therapeutic Efficacy of Immune Checkpoint Blockade Independent of BRCAness. *Cancer Res* 2019;79:311–9.
42 Zhu Q, Sharma N, He J, *et al*. USP7 deubiquitinase promotes ubiquitin-dependent DNA damage signaling by stabilizing RNF168*. *Cell Cycle* 2015;14:1413–25.
43 Wang A, Ning Z, Lu C, *et al*. USP22 Induces Cisplatin Resistance in Lung Adenocarcinoma by Regulating γH2AX-Mediated DNA Damage Repair and Ku70/Bax-Mediated Apoptosis. *Front Pharmacol* 2017;8:274.
44 Zhang D, Zaugg K, Mak TW, *et al*. A role for the deubiquitinating enzyme USP28 in control of the DNA-damage response. *Cell* 2006;126:529–42.
45 Luijsterburg MS, de Krijger I, Wiegant WW, *et al*. PARP1 Links CHD2-Mediated Chromatin Expansion and H3.3 Deposition to DNA Repair by Non-homologous End-Joining. *Mol Cell* 2016;61:547–62.
46 Wei B, Xu L, Guo W, *et al*. SHP2-Mediated Inhibition of DNA Repair Contributes to cGAS-STING Activation and Chemotherapeutic Sensitivity in Colon Cancer. *Cancer Res* 2021;81:3215–28.
47 Feng M, Jiang W, Kim BYS, *et al*. Phagocytosis checkpoints as new targets for cancer immunotherapy. *Nat Rev Cancer* 2019;19:568–86.